

pubs.acs.org/JPCC Article

Walk on a Flickering Path: Tracer Diffusion of Adsorbed O Atoms on a Ru(0001) Surface in the Limit of CO Saturation

Hannah Illner, Sung Sakong, Axel Gross, and Joost Wintterlin*



Cite This: https://doi.org/10.1021/acs.jpcc.5c04653



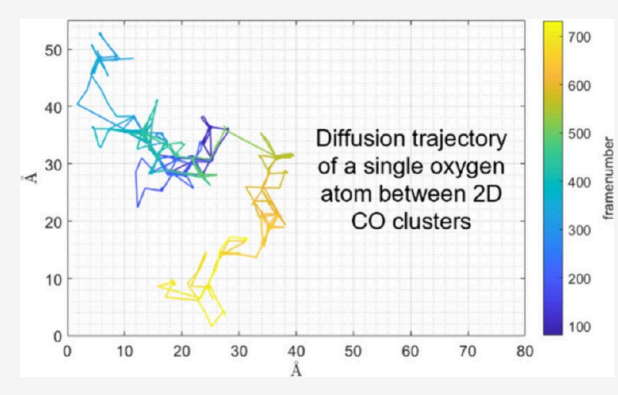
ACCESS I

Metrics & More

Article Recommendations

SI Supporting Information

ABSTRACT: Previous work has shown that tracer diffusion of adsorbed O atoms on a CO-covered Ru(0001) surface is driven by fluctuations of the CO clusters. Here, a study is presented on the question of whether this diffusion mechanism is suppressed at CO saturation. Experiments were performed using high-speed scanning tunneling microscopy (STM). Hopping rates of O atoms were extracted from atomic trajectories, and an activation energy was determined from temperature-dependent data. The energetics of the embedded O atoms in the CO layer was evaluated by density functional theory (DFT). DFT was also used to determine the structures occurring during the O/CO exchange process. CO at saturation forms densely packed 2D clusters on the Ru(0001) surface, which is known from previous work. The present STM data show that the trajectories of



the O atoms are restricted to the narrow gaps between the CO clusters but that the atoms still move by randomly hopping between neighboring hcp sites. The molecular structures of the clusters change as the O atoms move. Surprisingly, the mobility is higher than at lower CO coverages. DFT shows that, as an O atom jumps from an hcp site to a neighboring hcp site via an intermediate fcc site, several CO molecules at the edges of the clusters are displaced, leading to low-energy hopping pathways for the O atoms. The O atoms walk on "flickering paths" driven by fluctuations of the CO clusters. CO displacements cost more energy than at the lower coverages, but this effect is overcompensated by a reduced hopping barrier of the O atoms at the high CO coverage.

■ INTRODUCTION

Self-diffusion of adsorbed particles on a solid surface is a simple sequence of hopping events as long as the surface is largely empty and the particles only rarely collide with each other. In this limit, diffusion is described by a random walk of noninteracting single particles. However, in all applied surface processes, such as in heterogeneous catalysis, film growth, and electrode reactions, an adsorption layer is present and diffusion becomes complex. Even at low coverages, lateral interactions between the adsorbed particles play a role for diffusion, and at higher coverages collective site exchanges become dominant. ¹

Several scanning tunneling microscopy (STM) studies have shown how interactions between adsorbed particles may influence particle mobility on partially or fully covered surfaces. For example, at low coverages, O atoms adsorbed on a Ru(0001) surface and N atoms on an Fe(100) surface displayed hopping rates and directions that were considerably affected by interactions from single adsorbed atoms on neighboring sites. The influence of neighboring atoms extended over several lattice constants. When adsorbed particles formed small groups or islands, collective jumps were observed. For example, chains of CO molecules on a Cu(110) surface were more mobile than individual molecules.

On fully covered surfaces, diffusion of adsorbed particles is entirely mediated by collective processes. STM studies revealed

several tracer diffusion mechanisms that have analogs in 3D solids.⁵ For example, Pb atoms adsorbed on interstitial sites of a Ge(111) surface performed direct site exchanges with neighboring Ge atoms,⁶ a mechanism discussed for 3D solids (although usually regarded as unfavorable because of the high activation barrier).⁵ In and Pd atoms embedded in the top layer of a Cu(100) surface and Pb atoms in a Cu(111) surface moved by site exchanges with thermal vacancies in the terraces of the host lattices.^{7–10} A vacancy mechanism is the most frequent diffusion process in 3D solids.⁵ In an electrolyte solution, substitutional S atoms on a Br-covered Cu(100) surface showed exchange processes with neighboring Br atoms that resembled the so-called interstitialcy mechanism in 3D solids, and on the Cl-covered surface a ring-like exchange mechanism was observed, which is also known from 3D solids.^{5,11}

In previous work, we have investigated tracer diffusion of O atoms through a CO layer on a Ru(0001) surface by means of

Received: July 4, 2025 Revised: September 9, 2025 Accepted: September 12, 2025



STM, density functional theory (DFT), and kinetic Monte Carlo (kMC) simulations. 12,13 At a coverage of Θ = 0.33 monolayers (ML, defined as adsorbed particles per Ru surface atom), the CO molecules form an ordered $(\sqrt{3} \times \sqrt{3})R30^{\circ}$ structure. However, the diffusion of O atoms through this 2D solid has no analog in 3D solids but proceeds by, as we called it, a door-opening mechanism. It is based on the much higher jump rates of CO molecules than of the O atoms, leading to structural fluctuations of the CO layer around a minimum energy configuration. The fluctuations frequently open low-energy paths on which an O atom can jump to a neighboring site. After the O atom has jumped, neighboring CO molecules quickly rearrange to the minimum energy configuration, completing an O/CO site exchange. The process is efficient, and the O atoms move through the CO layer almost as fast as on the empty Ru surface. Mechanisms of this type, which are based on a flexible matrix of coadsorbed particles, may be relevant for catalytic reactions as they justify the assumption of microkinetic catalysis models that surface diffusion is fast and not rate-limiting, regardless of coverage.

We further demonstrated that the O diffusion rate on the Ru(0001) surface was even higher at an increased CO coverage (Θ = 0.47 ML). ¹⁴ The finding was explained by the disorder of the CO layer at this coverage, enabling yet faster fluctuations than in the ordered layer. In addition, the surface bonds of the O atoms are weakened by the stronger repulsive interactions between the O atoms and the CO molecules at the higher CO concentration. The O/CO site exchange still follows the dooropening mechanism, like in the ordered structure. In a further study, it was shown that O atoms at domain boundaries of the ($\sqrt{3} \ x \ \sqrt{3}$)R30° structure, where the layer is disordered in narrow, fluctuating stripes along the boundaries, move faster by one order of magnitude than in the ordered domains, confirming the role of fluctuations. ¹⁵

In all of these situations, a considerable fraction of the Ru atoms was empty, e.g., 2/3 of the sites in the $(\sqrt{3} \times \sqrt{3})R30^{\circ}$ CO structure. Fluctuations happen easily, and this can explain why the diffusion mechanism is different from the known mechanisms in 3D lattices. An open question was therefore how the mechanism changes when the Ru surface is saturated with CO. Here we present a study in which we have approached this problem by increasing the CO coverage to $\Theta = 0.66$ ML, the saturation coverage under ultrahigh vacuum (UHV) below ≈ 300 K.

CO at saturation forms a relatively complicated structure on the Ru(0001) surface that has been solved only recently. ¹⁶ The structure consists of approximately hexagonal arrays of compact, 2D clusters that contain between 7 and 19 molecules. In the clusters, the CO molecules are densely packed, forming a pseudo (1 x 1) structure. Because of repulsive interactions between the CO molecules, only the CO molecules at the center of a cluster are exactly at on top sites and in upright positions, whereas the outer molecules are laterally displaced and tilted away from the center. Between the clusters, single-atom-wide rows of Ru atoms are not permanently occupied by CO because the shifted and tilted molecules at the adjacent clusters restrict the space in these "corridors". The structure remains thermally stable up to the onset of CO desorption at \approx 300 K.

There appears to be hardly any free space for the fluctuationdriven diffusion of O atoms in this structure. One could, therefore, expect that the mechanism changes, possibly to one of the usual tracer diffusion mechanisms in 3D solids. Moreover, the mobility of the O atoms is expected to be reduced, possibly even to a degree that the high mobility assumption of catalytic reaction models breaks down. However, as we show here, this is not the case. The O atoms are even more mobile than at the lower CO coverages and also on the clean surface. Experiments were performed by high-speed STM. Atomic trajectories were obtained from which hopping rates of the O atoms were extracted. From temperature-dependent measurements, activation barriers were determined. DFT calculations were used to analyze the energetics of the structures involved in the O/CO site exchanges. We propose that all findings can be explained by the door-opening mechanism that remains valid even in the restricted space of the CO-saturated surface.

EXPERIMENTAL SECTION

Experiments were performed in a UHV chamber (base pressure $<1\times10^{-10}$ mbar) on an (0001)-oriented Ru single crystal. A home-built STM setup was used that can work at imaging rates of up to 50 frames per second and can be operated at sample temperatures between 50 and 500 K. 17 The UHV chamber is additionally equipped with an Auger electron spectrometer (AES), a low-energy electron diffraction (LEED) system, an ion gun for sputtering, a quadrupole mass spectrometer (QMS), and a sample manipulator.

For surface preparation, the Ru crystal was routinely treated by cycles of Ar sputtering (1 keV Ar $^+$ ions for 10–15 min at room temperature), flash annealing to 1470 K, oxidation to remove residual carbon (by dosing 2×10^{-7} mbar O_2 for 10–15 min at 910 K or, at lower carbon coverages, by dosing 2–20 L of O_2 at 298–423 K; 1 L = 1.33 \times 10 $^{-6}$ mbar s), and, finally, flash annealing to 1700 K. The cycles were repeated until the sample was clean according to AES. Because in AES the (strongly asymmetric) carbon KLL peak at 272 eV overlaps with the (symmetric) Ru MNN peak at 273 K, the coverage of residual C was determined indirectly, using the asymmetry of the experimental peak, which follows an established method. $^{18-20}$

Directly before an experiment, the sample was flash-annealed to 623 K to remove any readsorbed particles. A low amount of O_2 was dosed (0.03–0.05 L) at 370 K to prepare a surface with a low coverage of adsorbed O atoms. Then 50 L of CO were dosed at 345 K which does not yet lead to CO saturation but protects the sample from adsorption of contaminants from the residual gas during cooling. The sample was then transferred to the liquid He-cooled sample holder of the STM setup, and while the sample cooled to 70 K, another 15 L of CO were dosed. This procedure led to saturation with CO (Θ = 0.66 ML).

For a diffusion experiment, a certain temperature was set in a range between 225 and 268 K; the range was limited by the time resolution of the experiment. When the temperature was sufficiently constant, recording by STM was started. Images were taken in the high-speed, constant height mode of the STM at 10 frames per second. Movies consisting of several thousand STM images were recorded. The data were analyzed by means of a multiscale wavelet-based algorithm that identifies and tracks the mobile O atoms. ²¹ O hopping rates were extracted from the obtained trajectories.

COMPUTATIONAL DETAILS

To determine the potential energy surfaces (PES) of the adsorbed O atoms and CO molecules, periodic DFT calculations were performed by means of the VASP software package.²² The electronic wave functions were expanded up to 450 eV using a plane-wave basis set, and exchange-correlation

effects were computed using a revised version of the Perdew–Burke–Ernzerhof (RPBE) functional as suggested by Hammer and Nørskov.²³ The projector augmented wave (PAW) potential was employed to describe the ionic cores,²⁴ and Grimme's semiempirical D3 dispersion correction scheme was used for the van-der-Waals interactions between the adsorbed particles and between the adsorbates and the first layer of the Ru slab.^{25–29}

The Ru(0001) surface was modeled by slabs consisting of three atomic layers with optimized Ru bulk lattice parameters a = 2.74 Å and c/a = 1.58. The slabs were separated by vacuum layers of 15 Å, and a compensating dipole field was used to correct for the surface dipole. The structures of the adsorbates and of the topmost Ru layer were fully optimized for local energy minimum configurations with a force convergence criterion of 0.01 eV/Å.

To construct the configurations of the O atoms on the CO-covered surface, information from the previous study on the CO cluster structure of the pure CO layer was used. ¹⁶ Figure 1(a)

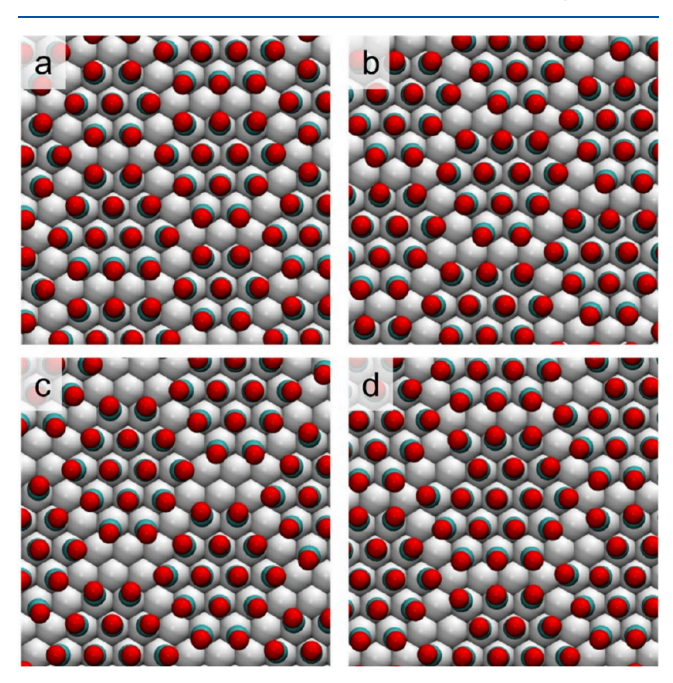


Figure 1. Four of the structure models treated by DFT. (a) Structure with two compact clusters of 12 CO molecules and one compact cluster of 7 CO molecules. (b) 12 CO cluster structure with twisted junctions. (c) 14 CO cluster structure with a vacancy block. (d) 18 CO cluster structure with a vacancy at a cluster edge. Red and turquoise spheres: CO molecules, gray spheres: Ru atoms. Further structures in Figure S1. [(a) is one of the models investigated in ref 16; coordinates available at 10.5281/zenodo.10784616].

shows, as an example, a configuration with two clusters of 12 CO molecules and one cluster of 7 CO molecules per unit cell. The model shows the on top positions of the center CO molecules, the displacements and tilts of the outer molecules, and the rows of empty Ru atoms ("corridors") between the clusters. The triangular CO configurations at the junction points of three corridors are particularly stable. Other cluster structures only differ in the number of CO molecules per cluster. ¹⁶

For oxygen, previous work has shown that the atom occupies an hcp site and that all three Ru atoms forming the hcp site have to be free of CO molecules. ^{12–14} Combining this condition with the structure elements of the CO clusters leads to three types of

configurations, in which the average CO coverages are comparable to the saturation coverages of the pure CO layer. In the first configuration [Figure 1(b)], shown for a 12 CO cluster structure, one corridor junction per unit cell still has a triangular configuration, but every other junction has a "twisted", chiral configuration that provides a CO-free hcp site for an O atom. In the second configuration [Figure 1(c)], shown for a 14 CO cluster structure, both triangular configurations at the junctions are lifted, giving configurations in which vacancies with more than one hcp site are grouped together ("vacancy block"). In the third configuration [Figure 1(d)], shown for an 18 CO cluster structure, one CO molecule has been removed from an edge position of an original 19 CO cluster, providing a CO-free hcp site in a corridor.

Using these structure elements, surface unit cells consisting of 14, 18, 19, 23, 24, 27, and 30 Ru atoms in the top layer were constructed [Figure 1 and Figure S1]. In cases where single Ru atoms were bare, in addition to the corridor, triangular junction, and twisted junction sites, we also considered modified CO clusters by adding extra CO molecules. The first Brillouin zones of the unit cells were integrated using 5x5x1, 5x5x1, 5x5x1, 4x4x1, 4x4x1, 4x4x1, and 3x3x1 k-point meshes for the respective surface unit cells.

Adsorption energies of the O atoms on the bare Ru(0001) surface were between -2.55 and -2.61 eV with respect to gas phase O_2 for all unit cells. These low variations, despite the different sizes of the unit cells, indicate that the interactions between the O atoms are relatively weak. Obviously, the unit cells treated here are large enough that the O atoms are sufficiently separated, so that O coverage effects on the energies could be disregarded.

The energies of the various structures were therefore treated in terms of the respective CO adsorption energies $E_{\rm ads}$. We define $E_{\rm ads}$ with respect to the energy of an isolated, adsorbed CO molecule on the bare Ru(0001) surface [eq 1]:

$$E_{\rm ads} = \frac{E_{\rm tot} - E_{\rm slab} - n_{\rm CO} E_{\rm CO}^{(g)}}{n_{\rm CO}} - E_{\rm CO}^*$$
 (1)

 $E_{\rm tot}$ is the total energy of a slab with adsorbed O atoms and CO molecules, $E_{\rm slab}$ is the energy of an uncovered Ru(0001) or O/Ru(0001) slab depending on the presence of an O atom, $E_{\rm CO}^{\rm (g)}$ is the energy of a CO molecule in the gas phase, $E_{\rm CO}^*$ is the energy of an isolated, adsorbed CO molecule on a (6 x 6) lattice on the Ru(0001) surface, and $n_{\rm CO}$ is the number of the CO molecules in the cell. $E_{\rm CO}^*$ is -1.89 eV in this setup, which overestimates the experimental value by 0.3 eV. 29 However, by referring to $E_{\rm CO}^*$, the adsorption energies $E_{\rm ads}$ only include the interactions between the adsorbed molecules; the overestimated adsorption energies of individual molecules cancel out. The activation barriers of the particle jumps were calculated by the nudged elastic band method with four images. 30

To support the interpretation of the STM data, constant height images were simulated using the Tersoff-Hamman approximation. Corresponding to the negative tunneling voltages (V_t) applied in the experiments, the densities of occupied states were integrated between the Fermi energy (0.0 eV) and energy values -0.2, -0.4, -0.5, -0.8, and -1.0 eV below E_F . Like in the previous study on the saturated, pure CO layer, the charges were calculated at distances between 1.6 and 3.6 Å above the O atoms of the CO layer in steps of 0.1 Å. Images were computed by linearly interpolating the charge grids.

The Journal of Physical Chemistry C

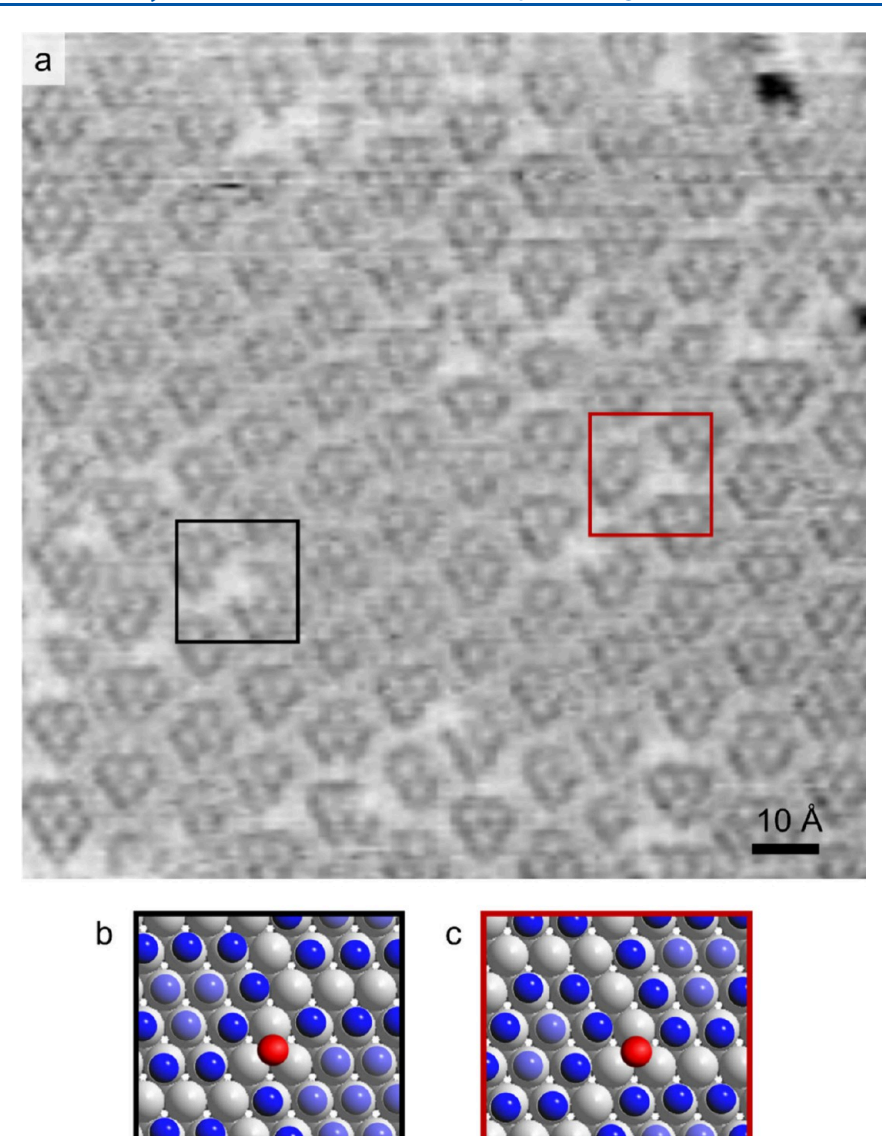


Figure 2. (a) STM image of the CO-saturated Ru(0001) surface (Θ = 0.66 ML) with embedded O atoms. Features with bright dots in the interiors and dark/bright rims are CO clusters, bright dots are O atoms. (The black feature is probably some carbon species.) T = 227 K, tunneling voltage (V_t) = -0.2 V, tunneling current (I_t) = 10 nA, constant height mode. (b) Model of the marked area in (a) with an O atom on a corridor site. (c) Model of the marked area in (a) with an O atom on a twisted junction site. Red spheres: O atoms; blue spheres: CO molecules; lighter blue spheres are the inner CO molecules that create the fine structure in the STM image; gray spheres: Ru atoms.

For an integration range of 0.0 to -1.0 eV and at a distance of 2.5 Å, the simulated images agreed well with the experimental data.

RESULTS AND DISCUSSION

Configuration of the Embedded O Atoms in the Saturated CO Layer. Figure 2(a) shows one frame from an STM movie recorded at 227 K on the saturated CO layer with embedded O atoms. One can see a roughly hexagonal pattern of features of various sizes, each displaying a few units of a hexagonal inner fine structure. The periodicity of the fine structure is ≈ 3.3 Å, slightly larger than the lattice constant of Ru(0001) of 2.70 Å. The features represent the compact, 2D CO clusters known from the saturated, pure CO layer, and the size variations reflect the variable numbers (7-19) of the CO molecules in the clusters. The fine structure reflects the inner CO molecules, and the more or less structureless space between the fine structure elements reflects the displaced and tilted outer

molecules. There is no contrast from the corridors between the clusters.

In addition to these features, several bright spots can be identified in Figure 2(a). These are absent on the pure CO layer and can therefore be interpreted as embedded O atoms. We mention that, in the constant current STM mode, adsorbed O atoms on metal surfaces usually appear dark, but in the constant height mode at negative tunneling voltages V_t the contrast is inverted. Similar images have been obtained in all experiments.

Figures 2(b) and (c) show schematic models of the two marked areas in Figure 2(a). The O atoms occupy 3-fold sites, consistent with the expected hcp sites, and the surrounding CO clusters show some differences to clusters without oxygen. In one case [Figure 2(b)], one CO molecule in a corridor is missing from the edge of a cluster, and the resulting CO-free hcp site is occupied by an O atom. In the second case [Figure 2(c)], a twisted junction site between three CO clusters is CO-free and

occupied by an O atom. These cases correspond to two configurations treated by DFT [Figure 1(b) and (d)].

Simulated STM images (Figure 3), confirm the models. Figure 3(a) shows a simulated image of a structure with clusters

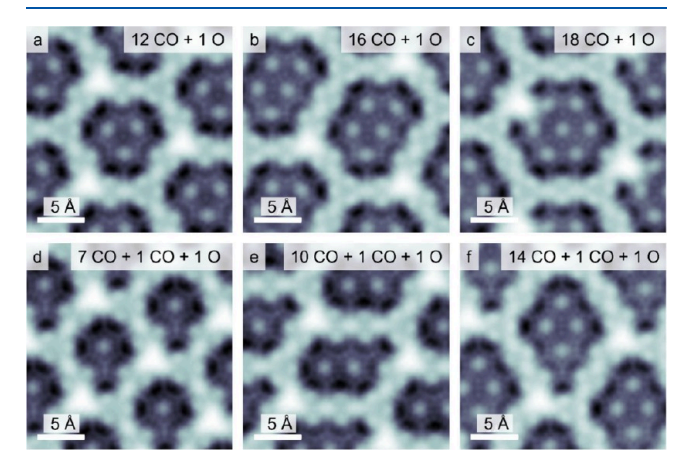


Figure 3. Simulated STM images of CO cluster structures with embedded O atoms. Inverted contrast like in the experiment; bright dots are at the positions of the inner CO molecules; bright intermediate spaces are at the positions of the outer CO molecules, and the brightest dots are at the positions of the O atoms. (a) and (c) Simulations of the models shown in Figure 1(b) and (d) with adsorbed O atoms on the CO-free hcp sites. (b) Simulation of one of the models shown in Figure S1. (d) to (f) Simulations of three of the models shown in Figure S1 with adsorbed O atoms and single additional CO molecules.

of 12 CO molecules [Figure 1(b)] and O atoms that occupy the twisted junction sites. The three central maxima in each unit of the simulated image are caused by the three inner CO molecules of the clusters, the weak modulation between the clusters is caused by the nine outer molecules, and there is no contrast

from the empty corridors. The bright spots at the corners of the unit cells are at the positions of the O atoms on the twisted junction sites. Figure 3(b) is equivalent, with 16 CO molecules per cluster and O atoms on the twisted junctions. Figure 3(c) is a simulation of a configuration with 18 CO molecules [the CO configuration of Figure 1(d)] with O atoms on the corridor sites. Figures 3(d) to (f) show configurations with embedded O atoms and single CO molecules added to sites in vacancy blocks. In all cases, the simulations are in good agreement with the experimental images.

Diffusion of the Embedded O Atoms. Movies recorded with the high-speed STM show that the embedded O atoms are mobile in the investigated temperature range (225 to 268 K). As an example, Figure 4 shows three images recorded with time intervals of 0.2 and 0.5 s on the same surface area, together with models of the marked areas (227 K). In the first frame, two O atoms (black and red arrows) occupy twisted junction sites with opposite chirality [Figure 4(a) and (d)]. In the second frame, the lower atom has moved to a corridor site, and the upper atom is still at the same position [Figure 4(b) and (e)]. At the same time, the number of CO molecules in the cluster below the displaced O atom has increased from 12 to 13. One CO molecule has left a site at the corridor (creating the CO-free hcp site for the O atom) and two originally empty Ru sites at the upper edge of the cluster are occupied by CO. There are further changes at the cluster above the displaced O atom. In the third frame, the lower O atom has jumped again, this time to a twisted junction site [Figure 4(c) and (f)] with opposite chirality to the original configuration [Figure 4(a) and (d)]. This jump is accompanied by changes in several clusters in the marked area which effectively create the CO-free hcp site for the O atom at the new twisted junction. The O atom thus moves by hopping between CO-free hcp sites, and during these jumps, the

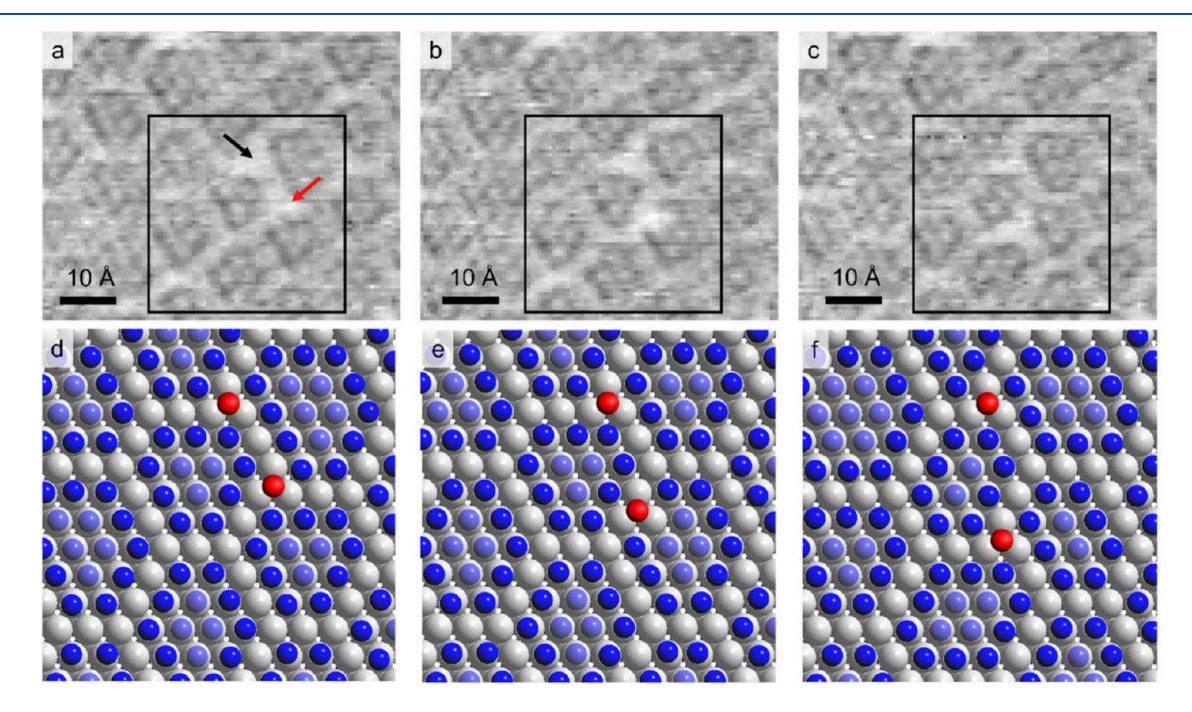


Figure 4. Series of STM images during jumps of an O atom. (a-c) STM images from a movie of the CO-saturated Ru(0001) surface $(\Theta = 0.66 \text{ ML})$ with embedded O atoms; all three images from the same area; time intervals between frames are 0.2 and 0.5 s. T = 227 K, $V_t = -0.2 \text{ V}$, $I_t = 10 \text{ nA}$, constant height mode, frame rate 10 s^{-1} , arrows mark two O atoms. (d-f) Models of the marked areas in (a-c). Red spheres: O atoms, blue spheres: CO molecules, gray spheres: Ru atoms.

The Journal of Physical Chemistry C

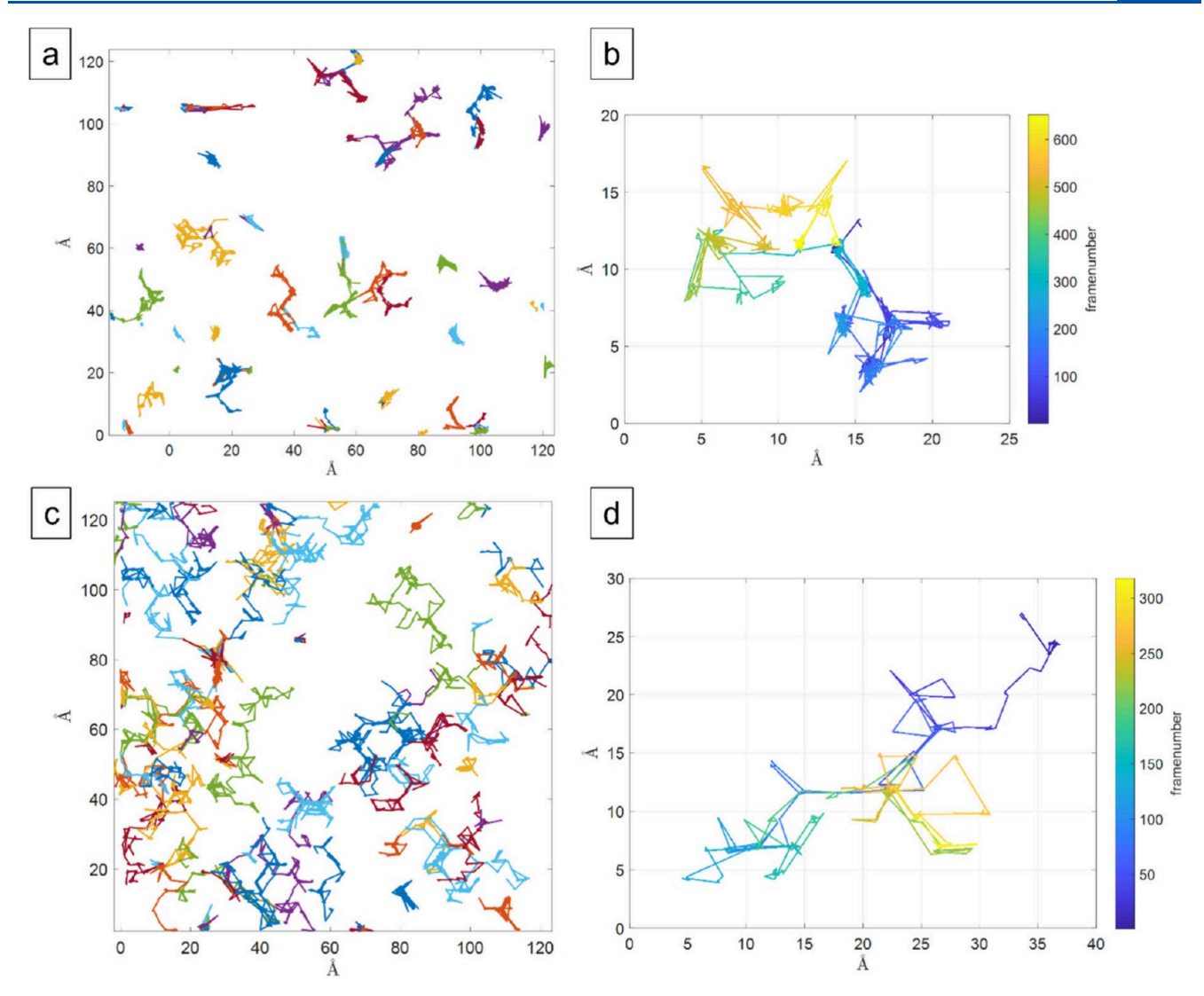


Figure 5. Trajectories of O atoms obtained with the tracking software. (a) All trajectories from an STM movie recorded at 245 K. $V_t = -0.2$ V, $I_t = 3$ nA, constant height mode, frame rate 10 s⁻¹. (b) Trajectory of a single O atom from the data set of (a). (c) All trajectories from an STM movie recorded at 259 K. $V_t = -0.2$ V, $I_t = 3$ nA, constant height mode, frame rate 10 s⁻¹. (d) Trajectory of a single O atom from the data set of (c).

molecules at the edges of several CO clusters change positions. (Movie S1 shows a full movie.)

Longer trajectories of the O atoms were recorded by means of the tracking software. Figure 5(a) and (c) shows, as examples, trajectories from a 652-frame movie at 244.5 K and from a 765frame movie at 259 K, respectively. (The data have been driftcorrected as described before.²¹) Colors mark trajectories of different O atoms or interrupted trajectories of given atoms when the tracking software has intermittently lost the atoms. As expected, the trajectories at 259 K are longer on average than at 244.5 K (the two movies cover about equal time periods). At the higher temperature, the trajectories display a characteristic honeycomb pattern, which obviously replicates the cluster structure of the CO layer. Such trajectory patterns have also been observed in experiments in which the CO structure was not well resolved. It can be concluded that the O atoms mainly move along the corridors between the junctions of the clusters and only rarely enter the interiors of the clusters. In Figure 5(c), the honeycomb pattern partially displays two parallel lines, indicating that the O atoms can travel along the corridors on two pathways. Despite the variations in cluster sizes and shapes,

their average positions remain unchanged over the periods of the STM movies.

Figure 5(b) and (d) shows trajectories of single O atoms from the data sets of Figure 5(a) and (c). Color codes represent time. At the lower temperature, the trajectory shows "nodes" of short lines which correspond to time periods in which the atom is found on the same adsorption site, and the number of visited sites is low. At the higher temperature, the atom spends less time on an adsorption site, often just the time of one frame, and the number of visited sites is higher. Jumps are mostly one lattice constant long; occasional longer displacements at the higher temperature can be explained by successive single jumps.

For statistical analysis of the trajectories the previously described procedure was applied. ¹² It includes checks that a bright feature identified by the software actually represents an O atom, and that trajectory sections in which two O atoms are more closely spaced than approximately 7 Å are removed. Data from altogether 15 temperatures in a range between 225 and 268 K were analyzed, each measurement consisting of several thousand STM images (Table S1). The results are displayed as displacement histograms between successive STM images. Figure 6(a) and (b) shows examples from two temperatures,

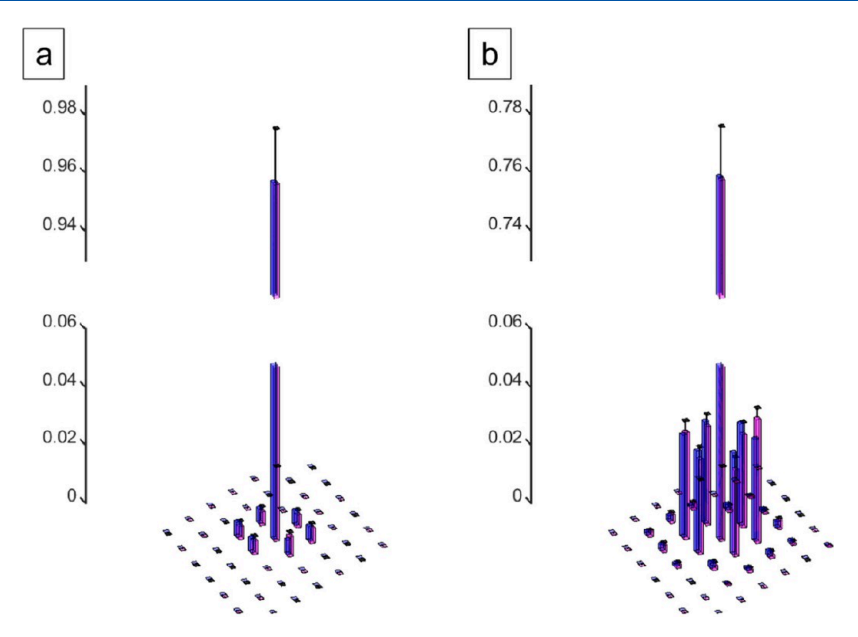


Figure 6. Displacement histograms of O atoms on the CO-saturated Ru(0001) surface. (a) and (b) from data sets at 234 and 261 K, respectively. Pink bars are from the experiments, blue bars from the fits with eq 3. Bar heights are relative counts of displacements from (x, y) = (0.0) to sites with coordinates x and y between successive images; the origins in (a) and (b) are at the highest bars.

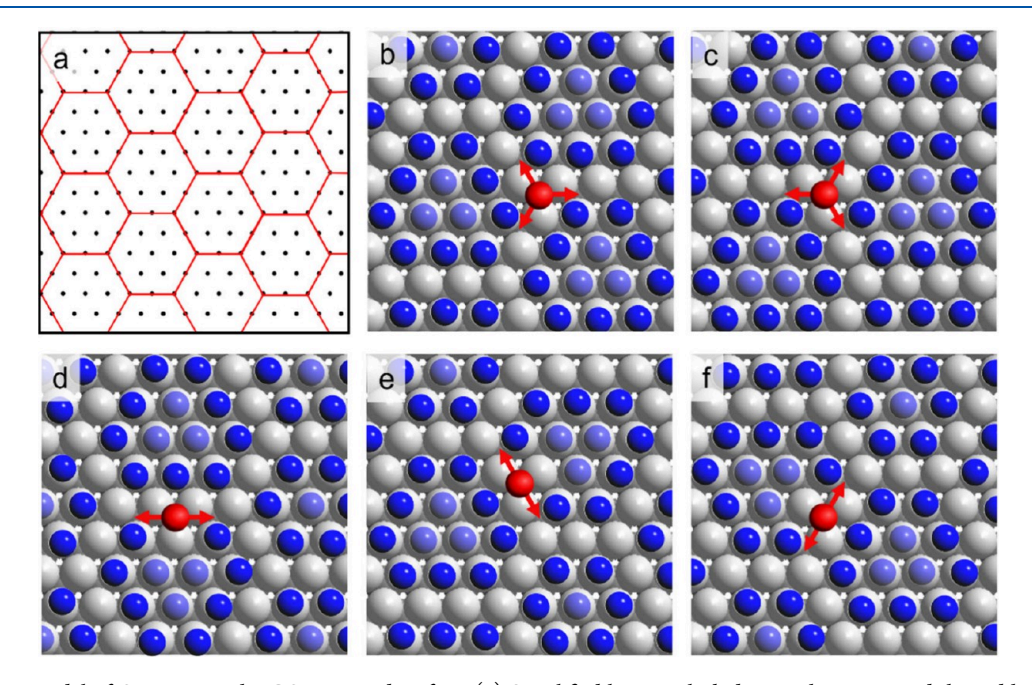


Figure 7. Diffusion model of O atoms on the CO-saturated surface. (a) Simplified lattice. Black dots are hcp sites, and the red honeycomb pattern marks hcp sites accessible to oxygen. (b-f) Structure models of the junctions and corridors of the cluster structure, respectively.

234 and 261 K (pink bars). As expected, the displacement distribution is broader and flatter at the higher temperature, but both histograms appear hexagonal.

Analysis of the Displacement Histograms. Like in the previous work, ^{12,14} the hopping probability of the O atoms was assumed to be given by a Poisson distribution [eq 2]

$$\tilde{P}_{t_0}(n) = \frac{(\Gamma t_0)^n}{n!} e^{-\Gamma t_0} \tag{2}$$

 $\tilde{P}_{t_0}(n)$ is the probability that an O atom jumps n times in the time period t_0 between two successive STM frames (0.1 s in the present case). To obtain an experimentally accessible quantity,

 $\tilde{P}_{t_0}(n)$ has to be multiplied by $w_n(x, y)$, the probability that an atom travels to a given site with coordinates (x, y) by a combination of n jumps. $w_n(x, y)$ is a geometry factor that depends on the symmetry of the lattice. It is evaluated by a recursion equation. Summing the product of $\tilde{P}_{t_0}(n)$ and $w_n(x, y)$ over all n gives $P_{t_0}(x, y)$, the probability that the O atom has moved to a site with coordinates (x, y) between two successive STM images. $P_{t_0}(x, y)$ corresponds to the experimental quantity plotted in the histograms.

For diffusion on a hexagonal lattice, $w_n(x, y)$ has a simple form.¹⁴ In the present case, the O atoms do not move on a hexagonal lattice, but on a partially ordered honeycomb network

defined by the CO clusters [Figure 5(c)]. A further complication is that the sizes and shapes of the clusters are not uniform and change with time. Including these effects in the setup of a recursion equation $w_n(x, y)$ in a precise way is not possible, but a simplified model lattice can at least capture basic elements of the actual process. The model we chose consists of a hexagonal lattice of hcp sites [Figure 7(a), black dots] superimposed by a periodic honeycomb network that defines the hcp sites that are actually accessible to the O atoms [Figure 7(a), red lines]. The honeycomb lattice reflects the experimental observation that the O atoms only occupy sites between the clusters, whereas the interiors of the clusters are largely excluded. Structure models of the two configurations at the junctions of this model lattice and of the three configurations at the corridors are shown in Figure 7(b,c) and (d-f), respectively. Size variations of clusters and the two parallel trajectories along the corridors were not included. The hopping rate Γ was assumed to be equal for all sites. The O paths on this network are treated irrespective of the fact that CO molecules have to be displaced for each jump event, as indicated by the arrows in Figure 7(b-f). These CO displacements are implicitly contained in the obtained hopping rates.

On this simplified lattice, recursion equations $w_n(x, y)$ can be formulated (SI). Five different geometry factors are obtained, one for each starting position on one of the five different types of sites on the honeycomb lattice. A difficulty for the analysis is that one cannot decide which of these sites is the respective starting position. The irregular shapes of the individual trajectories [Figure 5(b) and (d)] illustrate this problem. An averaging method was therefore applied (SI). It was assumed that the O atoms initially either occupy, with equal probability, one of the two different junction sites, so that the two corresponding geometry factors can be averaged to give an averaged geometry factor $w_n^{\rm jct}(x, y)$ for the junction sites. Or, the O atoms initially occupy, with equal probability, one of the three different corridor sites, and averaging the three corresponding geometry factors gives an averaged geometry factor $w_n^{\text{crd}}(x, y)$ for the corridor sites. Which fraction of atoms initially occupy junction sites or corridor sites was a priori not clear and left open. $P_{t_0}(x, y)$ is then given by eq 3:

$$P_{t_0}(x, y) = \sum_{n=0}^{\infty} \tilde{P}_{t_0}(n) [f w_n^{\text{jct}}(x, y) + (1 - f) w_n^{\text{crd}}(x, y)]$$
(3)

where $\tilde{P}_{t_0}(n)$ is taken from eq 2, and the expression in square brackets is the geometry factor for the honeycomb lattice. f is the fraction of atoms that initially occupy a junction site; we treat it as a second fitting parameter, in addition to the hopping frequency Γ contained in $\tilde{P}_{t_0}(n)$. Summing was performed up to n=10.

Figure 6(a) and (b) shows, as examples, fits of $P_{t_0}(x,y)$ (blue bars) to the experimental histograms at 234 and 261 K (pink bars). Very good agreement is found, and the residual plots correspondingly show low values (Figure S2). The agreement confirms the assumption of the model that the O atoms move by random jumps between neighboring adsorption sites. For the hopping rates, the fits give $\Gamma=0.3127~{\rm s}^{-1}$ and $\Gamma=2.7370~{\rm s}^{-1}$ at 234 and 261 K, respectively, and for the fraction of atoms at the initial junction sites, the fits give f=0.25 and 0.61, respectively. For comparison, we also performed fits with a recursion equation on a simple hexagonal lattice. The hopping rates, $\Gamma=0.3112~{\rm s}^{-1}$ and $\Gamma=2.6427~{\rm s}^{-1}$ at 234 and 261 K, respectively, are

almost identical to the values on the honeycomb lattice, indicating that the choice of the exact lattice and, thus, the simplifications of the model lattice, are uncritical. For all other measurements, application of eq 3 led to similar good fits to the experimental histograms. Table S1 lists the obtained Γ and f values. f shows no systematic trend with temperature, and the average over all measurements, $\langle f \rangle = 0.47 \pm 0.18$, indicates no significant difference between the occupation probabilities of the junction and corridor sites (the value for exact uniformity would be 2/5).

The hopping rates increase with temperature as shown in the Arrhenius plot (Figure 8). The plot contains measurements

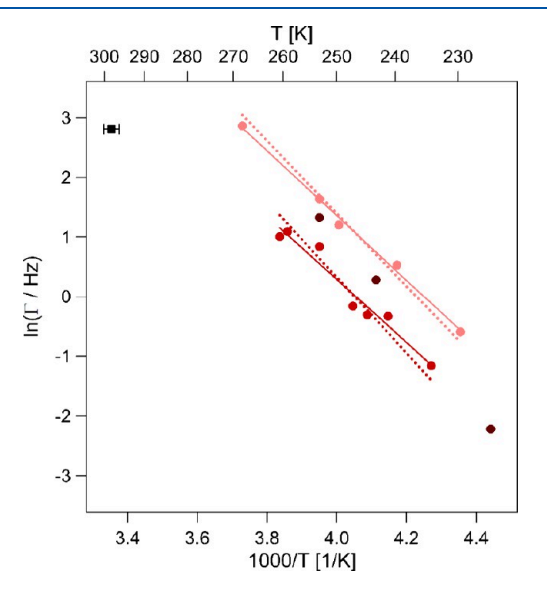


Figure 8. Arrhenius plot of hopping frequencies of O atoms on the CO-saturated Ru(0001) surface. Red and pink data points are from two separate experiments, linear regressions shown as full lines, and dark red data points are from a control experiment with a higher O coverage. Dotted lines are linear regressions with preexponential factor Γ^0 fixed at $10^{11.2}~\text{s}^{-1}$. Black square: data point from adsorbed O atoms on the bare Ru(0001) surface at room temperature, taken from ref.²

from two separate full experiments (red and pink data points) and three data points from a control experiment with a higher O coverage (dark red data points). That the two full data sets are displaced with respect to each other, despite nominally identical conditions, is probably caused by an error in the reference temperatures. However, both sets are well fitted by linear regressions (solid lines), giving almost identical activation energies, $E^* = 0.46 \pm 0.04$ eV and 0.47 ± 0.02 eV, respectively, and preexponential factors, $\Gamma^0 = 10^{9.3 \pm 0.9}$ s⁻¹ and $10^{10.0 \pm 0.4}$ s⁻¹, respectively. The hopping rates from the control experiment are in the same range, demonstrating that the method of excluding too closely spaced O atoms works well. We additionally applied linear regressions with fixed preexponential factors at $\Gamma^0 = 10^{11.2}$ s⁻¹, the average value from previous experiments at 0.33 ML of CO where a higher number of data points was available. 12 With this constraint, the linear regressions still fit the data well (Figure 8, dotted lines), but the activation energies increase somewhat, to $E^* = 0.55$ and 0.53 eV, respectively.

Table 1 relates the Arrhenius parameters to the parameters from the previous work. At CO saturation ($\Theta = 0.66$ ML), the experimental activation energies are in the same range as at 0.47 ML, and with the fixed preexponential factor they are somewhat lower. They are distinctly lower than at 0.33 ML, independently

Table 1. Activation Energies and Preexponential Factors as Functions of CO Coverage^a

Θ [ML]	exp. E* [eV] for O jump	exp. Γ^0 [s ⁻¹] for O jump	exp. E^* [eV] for O jump with fixed Γ^0 at $10^{11.2}$ s ⁻¹	$E_{\rm a,CO}$ [eV] for initial CO displ., DFT	$E_{\rm d,CO}$ [eV] of config. with displ. CO, DFT	$E_{\text{a,ox}}$ [eV] for O jump after displ. CO, DFT	E _{tst} [eV], DFT	ref
0.33	0.63 ± 0.03	$10^{11.1 \pm 0.7}$	0.64	0.30	0.16	0.62	0.78	12, 13
0.47	0.44 ± 0.04	$10^{8.9 \pm 0.8}$	0.56	0.25-0.33	0.06-0.15	0.55-0.56	0.65 - 0.73	14
0.66/0.63	0.46 ± 0.04	$10^{9.3 \pm 0.9}$	0.55	0.26	0.24	0.45	0.69	this
0.66/0.63	0.47 ± 0.02	$10^{10.0 \pm 0.4}$	0.53	0.20	0.24	0.43	0.09	work

"Experimental activation energies E^* , preexponential factors Γ^0 and activation energies with fixed preexpontential factor at $\Gamma^0=10^{11.2}~{\rm s}^{-1}$. DFT-calculated activation energies for the initial CO excitation $E_{a,\rm CO}$ and calculated energies of the excited states $E_{d,\rm CO}$. DFT-calculated activation energies $E_{a,\rm ox}$ for the jump of an O atom to a CO-free fcc site after displacement of a CO molecule. Total energies $E_{\rm tst}$ of the transition states with respect to the minimum energy configurations. ($E_{\rm tst}$ is not in all cases exactly the sum of $E_{\rm d,CO}$ and $E_{\rm a,ox}$ when some following steps are energetically higher.) The two coverage values 0.66 and 0.63 ML in the last two rows are from the experiment and from the calculations, respectively.

ı

of the preexponential factor. (For 0.33 ML there are two different jump processes; we here only consider the one connected with an actual O/CO site exchange. (12,13) The preexponential factors only show small differences. Equivalently, the absolute hopping rates at CO saturation (table S1) are in the same range or somewhat higher than at 0.47 ML, and they are distinctly higher than at 0.33 ML. (12,14) When we extrapolate the regression lines in the Arrhenius plot to room temperature—here a data point exists for O atoms on the bare Ru(0001) surface (Figure 8, black data point) —then we find that the hopping rate on the CO-saturated is even higher than on the CO-free surface. Quite surprisingly, the mobility of the embedded O atoms on the CO-saturated surface is not only not reduced but even enhanced compared to lower coverages and also to the bare surface.

DFT Calculations. DFT calculations were performed to explain this result. Figure 9 depicts the calculated energies [as CO adsorption energies $E_{\rm ads}$, eq 1] of all considered CO cluster structures with and without coadsorbed O atoms as a function of CO coverage. All values are positive because $E_{\rm ads}$ is relative to an isolated adsorbed CO molecule and there are repulsive

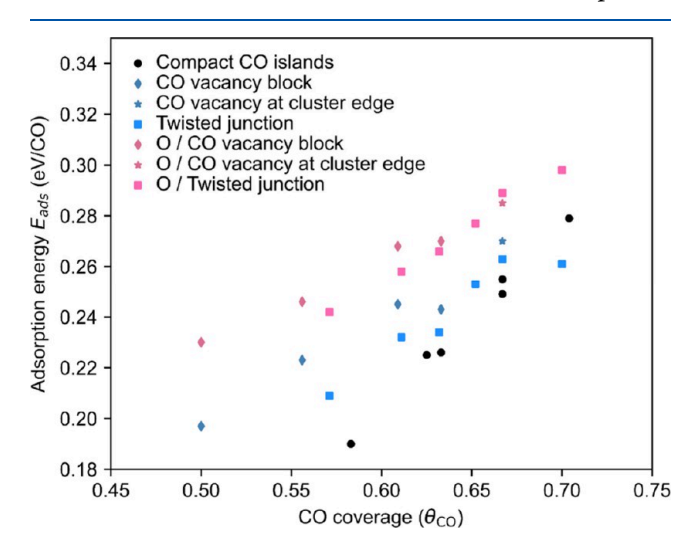


Figure 9. Energies of structures vs CO coverage from the DFT calculations. Black dots: compact, pure CO cluster structures (almost the same values as in ref 16; slight offsets are explained by a somewhat different setup of the calculations); blue squares: pure CO structures with twisted junctions; blue diamonds: pure CO structures with vacancy blocks; blue star: pure CO structure with vacancies at cluster edges; red squares: structures with O atoms on twisted junction sites; red diamonds: structures with O atoms on vacancy block sites; red star: structure with O atoms on vacancy sites at the cluster edges.

interactions in all structures. Without O atoms, compact CO cluster structures (black dots) are the most stable configurations at a given CO coverage, as previously reported. 16 (This is except for the data at $\Theta \approx 0.7$ ML, which is beyond the experimental saturation coverage.) Cluster structures with bare hcp sites (examples are shown in Figure 1) are less stable (blue data points). This difference is explained by the fact that in order to create a bare hcp site at a given CO coverage, one has to concentrate the molecules into larger clusters, which generally lowers the adsorption energy per CO molecule. 16 Within the structures with bare hcp sites, twisted junction configurations (blue squares) are more stable than vacancy block configurations (blue diamonds). This fact suggests that one can modify the shape of a cluster by putting CO molecules on sites that are different from sites in the corridors, triangular junctions, or twisted junctions. A configuration with a bare hcp site at a cluster edge (blue star) is similarly stable as the twisted junction configuration for the same cluster size of 18 CO molecules (Θ = 0.67 ML).

With O atoms on the CO-free hcp sites, all energies increase (red data points), a result of the relatively strong repulsion between O and the CO molecules. Configurations with O atoms on the twisted junctions (red squares) are more stable than configurations with O atoms in the vacancy blocks (red diamonds); the difference is more pronounced at low coverages. As shown for two 18 CO cluster structures ($\Theta = 0.67$ ML), the energy of a configuration with O atoms at corridor sites (red star) is comparable to the configuration with O atoms at twisted junction sites (red square). This fact is in agreement with the experimental finding that the occupation probabilities of the junction and corridor sites [expressed by the factor f in eq 3] are about the same.

To probe the dynamics of the O jumps, a 12 CO twisted junction structure (Θ = 0.63 ML), with an O atom on the COfree hcp site, was chosen as starting configuration (Figure 10, first model, O_{hcp}/12CO). It is a local energy minimum, and there are no CO-free 3-fold sites to which the O atom can jump. To create a CO-free site, one of the neighboring CO molecules is displaced to a corridor site (Figure 10, second model). The activation energy, $E_{a,CO} = 0.26$ eV, is comparable to the value at 0.47 ML and marginally lower than at 0.33 ML (Table 1). The energy $E_{\rm d,CO}$ of the resulting $O_{\rm hcp}/12{\rm CO}^{(a)}$ configuration is 0.24 eV higher than the starting configuration. This increase is significantly higher than at the lower coverages (Table 1), but this is what is expected as the CO molecule has to be placed on a site in the narrow corridor where the repulsion by the neighboring CO molecules is strong. The barrier to move the CO molecule back is only 0.02 eV. It can, therefore, be assumed that the initial excitation of the CO structure is in equilibrium.

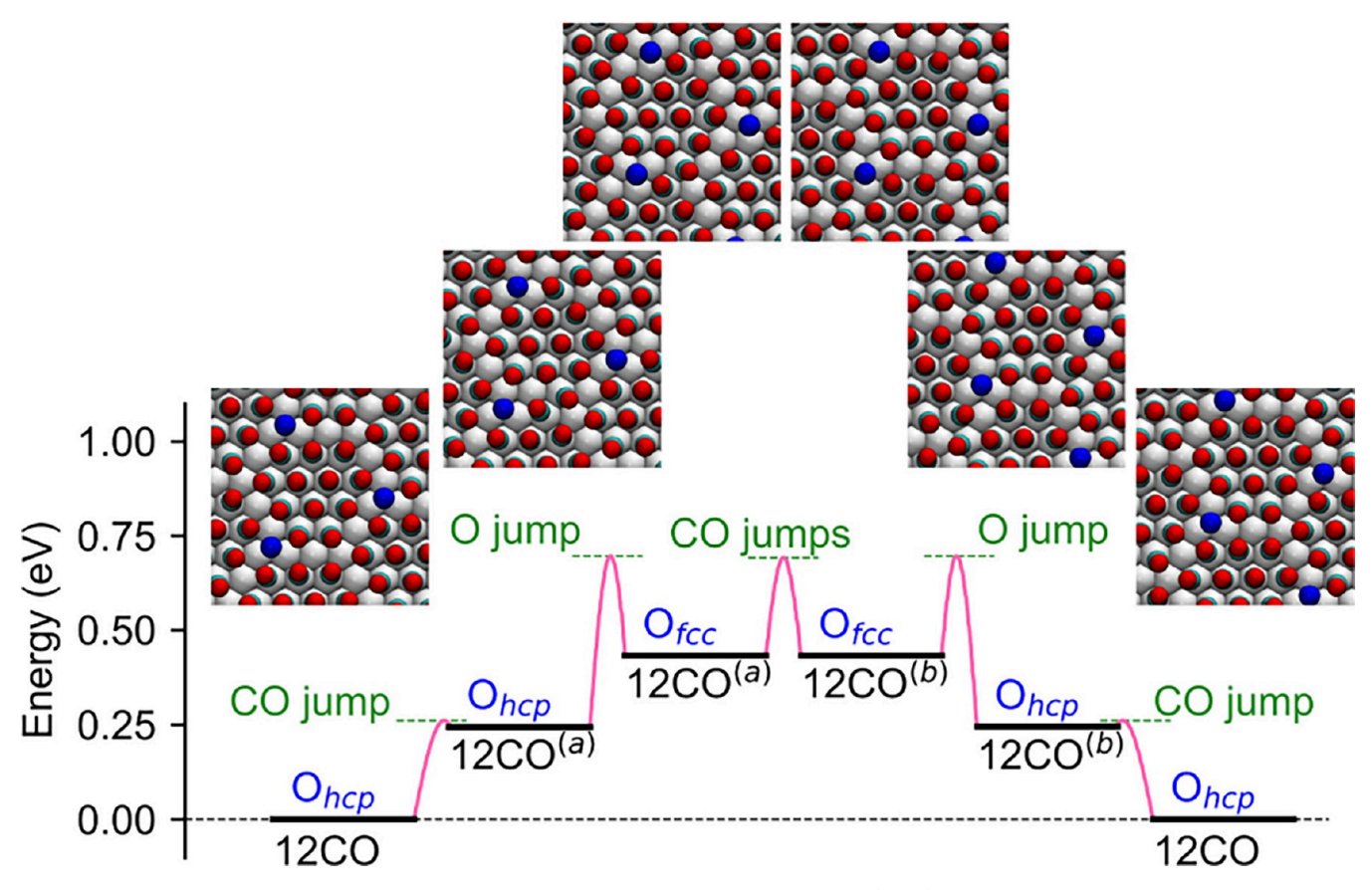


Figure 10. Energy diagram of an hcp \rightarrow fcc \rightarrow hcp jump of an O atom on the CO-saturated Ru(0001) surface. Models correspond to the six levels on the energy profile; oxygen atoms are indicated as blue spheres, otherwise same color code as in Figure 1.

By displacing the CO molecule, a channel to a CO-free fcc site has been opened. One could, additionally, create a CO-free hcp site, but then two CO molecules have to be displaced, which costs 0.54 eV, making this sequence less probable. More likely is that the O atom first jumps to the CO-free fcc site (Figure 10, third model, $O_{fcc}/12 \text{ CO}^{(a)}$). The activation energy for this step, $E_{\rm a,ox}$ = 0.45 eV, is distinctly lower than at the lower CO coverages (Table 1). We explain this fact by the changing distances between the CO molecules and the O atom along the path of the jump. In the $O_{hcp}/12CO^{(a)}$ configuration, the distances between the CO molecules and the O atom are, on average, shorter than in the transition state (which is approximately the bridge site between the hcp and the fcc sites). Hence, as the O atom moves from the energy minimum to the transition state, the repulsion by the CO molecules and thus the activation energy decreases. Such an effect also occurred at $\Theta = 0.47$ ML, ¹⁴ but in the present case the effect is stronger because of the higher CO coverage. For the absolute energy of the transition state E_{tst} the two effects of the high CO coverage, an increase of $E_{d,CO}$ and a decrease of $E_{a,ox}$, partially cancel out, but the decrease of $E_{a,ox}$ is higher than the increase of $E_{\rm d,CO}$. The resulting value, 0.69 eV, is therefore lower than at the lower coverages (Table 1).

From the $O_{fcc}/12CO^{(a)}$ configuration, the O atom could then jump back to the original site, or several CO molecules rearrange in several consecutive random steps, each with a slightly lower activation energy than for the back jump, to give the configuration $O_{fcc}/12CO^{(b)}$ (Figure 10, fourth model). It has the same symmetry and optimized structure and energy as the $O_{fcc}/12CO^{(a)}$ configuration. From there, the O atom can jump to a neighboring CO-free hcp site (the $O_{hcp}/12CO^{(b)}$

configuration, Figure 10, fifth model). Finally, one CO displacement leads to a new energy minimum configuration (Figure 10, sixth model), which is equivalent to the starting configuration. As a result, the O atom has moved by one lattice constant between two hcp sites. In the intermediate states of this process, when the O atom is on the fcc site and the CO molecules rearrange quickly, the outcome can, of course, be different and lead to a different final configuration, e.g., one in which the O atom is on an hcp site in a corridor. (In the experiment, this is the more likely result as the O atoms move along the corridors.) In any case, the scenario is based on fluctuations in the CO layer and follows the door-opening mechanism known from the lower coverages; it only differs with respect to the detailed excitations of the CO layer.

The scenario is in agreement with the experimental observations. The experiments have shown that the motion of the O atoms is correlated with changes in the positions of CO molecules at the cluster edges. The fact that the experimental trajectories only show O atoms on hcp sites is consistent with the high energy of the intermediate fcc site and the corresponding short lifetime. The calculated energy of the transition state maximum E_{tst} is somewhat higher than the experimental activation energies E^* , but this has similarly been found at the lower coverages (Table 1). (Because of the preequilibrium of the initial CO fluctuation, the experimental E^* corresponds to E_{tst} which contains the energy to create the configuration with the displaced CO, $E_{d,CO}$.) When the experimental activation energy is corrected for a fixed preexponential factor, then the agreement is quite reasonable. Moreover, the calculations reproduce the experimentally

observed trend that the activation energies decrease with increasing CO coverage (Table 1). In sum, the increased mobility on the CO-saturated layer can be explained by two counteracting effects: Fluctuations are made more difficult by the restricted space in the saturated layer, but at the same time the jump barrier is lowered by the increased repulsive interactions between the O atoms and CO molecules, and this effect predominates.

CONCLUSIONS

Adsorbed O atoms on a Ru(0001) surface which is covered with a saturated layer of CO molecules ($\Theta=0.66~\mathrm{ML}$) are highly mobile. High-speed STM movies recorded at temperatures between 225 and 268 K reveal that the O atoms perform random jumps between neighboring adsorption sites, like on the empty surface and at lower CO coverages. In contrast to these situations, the atomic trajectories are restricted to the gaps between the close-packed clusters of CO molecules that form the saturated layer. When O atoms move in these gaps, the jumps are accompanied by site changes of CO molecules at the edges of several adjacent clusters. Despite the narrow space between the clusters, the mobility is even higher than at lower CO coverages, because the activation energy for the jumps of the O atoms in the multidimensional potential energy surface is lower

The energy profile obtained by DFT shows that a jump event of an O atom is initiated by displacing a CO molecule to an unfavorable site between the clusters. In this way, a path is opened on which the O atom can jump from its hcp site to an empty fcc site. Random rearrangements involving several successive CO jumps can then create a path to an empty neighboring hcp site. After the O atom has jumped to this site, further CO displacements restore a stable configuration. The process can be seen as a walk on a "flickering path", driven by CO fluctuations between the clusters. It is quite similar to the dooropening mechanism previously derived for lower CO coverages. At the high CO coverage, repulsions between the O atoms and the CO molecules are higher, which alters the energy landscape from that at the lower coverages, giving a lower activation energy and an increased mobility.

We can conclude that the assumption of a high, not ratelimiting diffusion of adsorbed particles, the basis of microkinetic models of catalytic reactions, is valid up to saturation of the adsorption layer. We have shown this for the specific example of tracer diffusion of O atoms on a CO-saturated Ru(0001) surface, but similar systems, such as the cluster structure formed at 0.70 ML of CO on the Ir(111) surface, 33 can be expected to show the same effect. In how far this conclusion can be generalized is not an easy question to answer. The "flickering path" process is based on the fact that even the saturated CO layer still constitutes a "soft grid" that facilitates easy fluctuations. Adsorption systems that contain sufficient numbers of empty sites may be predicted to show similar effects. When we restrict ourselves to tracer diffusion of coadsorbed particles in layers of adsorbed CO molecules, we find that the van-der-Waals diameter of CO is larger than the lattice constants of all usual low-index metal surfaces. Coverages of 1.00 ML, conditions under which molecular displacement should, in fact, be suppressed, are generally not accessible, even at high pressures. On the other hand, CO at saturation can form other types of structures than clusters, e.g., moiré structures in which the molecules form close-packed layers that display a lattice mismatch with the underlying metal surfaces. Such structures

have, e.g., been observed for CO on Pt(111) and Co(0001) surfaces. Surfaces. Coverages are comparable to the cluster structures, but because of the uniform spacings between the CO molecules in such layers, there are no defined empty adsorption sites that are required for the type of fluctuation-driven mechanism described here. Fluctuations may still be possible, but these probably happen in the form of homogeneous compressions of the CO layers. It might be interesting to see how tracer diffusion of coadsorbed atoms is affected in such cases.

ASSOCIATED CONTENT

Supporting Information

The Supporting Information is available free of charge at https://pubs.acs.org/doi/10.1021/acs.jpcc.5c04653.

Models of CO structures with and without O atoms treated by DFT and used for the data of Figure 9. Residual plots of the displacement histograms of Figure 6. Table of STM data used for the Arrhenius plot in Figure 8. Derivation of eq 3 (PDF)

STM movie of diffusing oxygen atoms on the CO-saturated Ru(0001) surface T = 247 K (AVI)

AUTHOR INFORMATION

Corresponding Author

Joost Wintterlin — Department of Chemistry, Ludwig-Maximilians-Universität München, 81377 Munich, Germany; Center for NanoScience, 80799 Munich, Germany; orcid.org/0000-0002-0636-7538; Email: wintterlin@cup.uni-muenchen.de

Authors

Hannah Illner — Department of Chemistry, Ludwig-Maximilians-Universität München, 81377 Munich, Germany; orcid.org/0000-0002-9559-1821

Sung Sakong – Institute of Theoretical Chemistry, Universität Ulm, 89081 Ulm, Germany; ⊚ orcid.org/0000-0001-9777-7489

Axel Gross – Institute of Theoretical Chemistry, Universität Ulm, 89081 Ulm, Germany; orcid.org/0000-0003-4037-7331

Complete contact information is available at: https://pubs.acs.org/10.1021/acs.jpcc.5c04653

Notes

The authors declare no competing financial interest.

ACKNOWLEDGMENTS

The authors acknowledge support by the Dr. Barbara Mez-Starck Foundation and the computational resources provided by the federal state of Baden-Württemberg through the bwHPC initiative and by the German Science Foundation (DFG) under Grant No. INST40/575-1 FUGG (JUSTUS 2 cluster).

REFERENCES

- (1) Barth, J. V. Transport of adsorbates at metal surfaces: From thermal migration to hot precursors. *Surf. Sci. Rep.* **2000**, *40*, 75–149. (2) Renisch, S.; Schuster, R.; Wintterlin, J.; Ertl, G. Dynamics of adatom motion under the influence of mutual interactions: O/Ru(0001). *Phys. Rev. Lett.* **1999**, *82*, 3839–3842.
- (3) Pedersen, M. Ø.; Österlund, L.; Mortensen, J. J.; Mavrikakis, M.; Hansen, L. B.; Stensgaard, I.; Lægsgaard, E.; Nørskov, J. K.; Besenbacher, F. Diffusion of N adatoms on the Fe(100) surface. *Phys. Rev. Lett.* **2000**, *84*, 4898–4901.

- (4) Briner, B. G.; Doering, M.; Rust, H.-P.; Bradshaw, A. M. Microscopic molecular diffusion enhanced by adsorbate interactions. *Science* 1997, 278, 257–260.
- (5) Mehrer, H. Diffusion in Solids, 1st. ed.; Springer: Berlin, Heidelberg, 2007.
- (6) Ganz, E.; Theiss, S. K.; Hwang, I.-S.; Golovchenko, J. Direct measurement of diffusion by hot tunneling microscopy: Activation energy, anisotropy, and long jumps. *Phys. Rev. Lett.* **1992**, *68*, 1567–1570.
- (7) van Gastel, R.; Somfai, E.; van Saarloos, W.; Frenken, J. W. M. A giant atomic slide-puzzle. *Nature* **2000**, 408, 665–665.
- (8) van Gastel, R.; Somfai, E.; van Albada, S. B.; van Saarloos, W.; Frenken, J. W. M. Nothing moves a surface: Vacancy mediated surface diffusion. *Phys. Rev. Lett.* **2001**, *86*, 1562–1565.
- (9) Grant, M. L.; Swartzentruber, B. S.; Bartelt, N. C.; Hannon, J. B. Diffusion kinetics in the Pd/Cu(001) surface alloy. *Phys. Rev. Lett.* **2001**, *86*, 4588–4591.
- (10) Anderson, M. L.; D'Amato, M. J.; Feibelman, P. J.; Swartzentruber, B. S. Vacancy-mediated and exchange diffusion in a Pb/Cu(111) surface alloy: Concurrent diffusion on two length scales. *Phys. Rev. Lett.* **2003**, *90*, No. 126102.
- (11) Rahn, B.; Wen, R.; Deuchler, L.; Stremme, J.; Franke, A.; Pehlke, E.; Magnussen, O. M. Coadsorbate-induced reversal of solid-liquid interface dynamics. *Angew. Chem., Int. Ed.* **2018**, *57*, 6065–6068.
- (12) Henß, A.-K.; Sakong, S.; Messer, P. K.; Wiechers, J.; Schuster, R.; Lamb, D. C.; Groß, A.; Wintterlin, J. Density fluctuations as door-opener for diffusion on crowded surfaces. *Science* **2019**, *363*, 715–718.
- (13) Sakong, S.; Henß, A.-K.; Wintterlin, J.; Groß, A. Diffusion on a crowded surface: kMC simulations. *J. Phys. Chem. C* **2020**, *124*, 15216–15224
- (14) Illner, H.; Sakong, S.; Henß, A.-K.; Groß, A.; Wintterlin, J. Diffusion of O atoms on a CO-covered Ru(0001) surface—a combined high-speed scanning tunneling microscopy and density functional theory study at an enhanced CO coverage. *J. Phys. Chem. C* **2023**, *127*, 7197—7210.
- (15) Kügler, A.-K.; Illner, H.; Wintterlin, J. An STM study on the diffusion of O atoms on a CO-covered Ru(0001) surface—the role of domain boundaries. *Surf. Sci.* **2025**, *751*, No. 122597.
- (16) Illner, H.; Sakong, S.; Groß, A.; Wintterlin, J. Solution of the structure of the high-coverage CO layer on the Ru(0001) surface—a combined study by density functional theory and scanning tunneling microscopy. *J. Chem. Phys.* **2024**, *161*, 014703.
- (17) Henß, A. K.; Wiechers, J.; Schuster, R.; Platschkowski, V.; Wintterlin, J. A beetle-type, variable-temperature scanning tunneling microscope for video-rate imaging. *Jpn. J. Appl. Phys.* **2020**, *59*, No. SN1007.
- (18) Goodman, D. W.; White, J. M. Measurement of active carbon on ruthenium (110): Relevance to catalytic methanation. *Surf. Sci.* **1979**, 90, 201–203.
- (19) van Staden, M. J.; Roux, J. P. The superposition of carbon and ruthenium auger spectra. *Appl. Surf. Sci.* **1990**, *44*, 259–262.
- (20) Marchini, S.; Günther, S.; Wintterlin, J. Scanning tunneling microscopy of graphene on Ru(0001). *Phys. Rev. B* **2007**, *76*, No. 075429.
- (21) Messer, P. K.; Henß, A. K.; Lamb, D. C.; Wintterlin, J. A multiscale wavelet algorithm for atom tracking in STM movies. *New J. Phys.* **2022**, *24*, No. 033016.
- (22) Kresse, G.; Furthmüller, J. Efficient iterative schemes for ab initio total-energy calculations using a plane-wave basis set. *Phys. Rev. B* **1996**, 54, 11169–11186.
- (23) Hammer, B.; Hansen, L. B.; Nørskov, J. K. Improved adsorption energetics within density-functional theory using revised Perdew-Burke-Ernzerhof functionals. *Phys. Rev. B* **1999**, *59*, 7413–7421.
- (24) Blöchl, P. E. Projector augmented-wave method. *Phys. Rev. B* **1994**, *50*, 17953–17979.
- (25) Grimme, S.; Antony, J.; Ehrlich, S.; Krieg, H. A consistent and accurate ab initio parametrization of density functional dispersion correction (DFT-D) for the 94 elements H-Pu. *J. Chem. Phys.* **2010**, 132, No. 154104.

- (26) Grimme, S. Density functional theory with London dispersion corrections. *Wiley Interdiscip. Rev.: Comput. Mo. Sci.* **2011**, *1*, 211–228.
- (27) Sakong, S.; Forster-Tonigold, K.; Groß, A. The structure of water at a Pt(111) electrode and the potential of zero charge studied from first principles. *J. Chem. Phys.* **2016**, *144*, No. 194701.
- (28) Sakong, S.; Groß, A. The importance of the electrochemical environment in the electro-oxidation of methanol on Pt(111). ACS Catal. 2016, 6, 5575–5586.
- (29) Mahlberg, D.; Sakong, S.; Forster-Tonigold, K.; Groß, A. Improved DFT adsorption energies with semiempirical dispersion corrections. *J. Chem. Theory Comput.* **2019**, *15*, 3250–3259.
- (30) Henkelman, G.; Jónsson, H. Improved tangent estimate in the nudged elastic band method for finding minimum energy paths and saddle points. *J. Chem. Phys.* **2000**, *113*, 9978–9985.
- (31) Tersoff, J.; Hamann, D. R. Theory of the scanning tunneling microscope. *Phys. Rev. B* **1985**, *31*, 805–813.
- (32) Wintterlin, J.; Trost, J.; Renisch, S.; Schuster, R.; Zambelli, T.; Ertl, G. Real-time STM observations of atomic equilibrium fluctuations in an adsorbate system: O/Ru(0001). *Surf. Sci.* **1997**, *394*, 159–169.
- (33) Ueda, K.; Suzuki, K.; Toyoshima, R.; Monya, Y.; Yoshida, M.; Isegawa, K.; Amemiya, K.; Mase, K.; Mun, B. S.; Arman, M. A.; et al. Adsorption and reaction of CO and NO on Ir(111) under near ambient pressure conditions. *Top. Catal.* **2016**, *59*, 487–496.
- (34) Longwitz, S. R.; Schnadt, J.; Vestergaard, E. K.; Vang, R. T.; Lægsgaard, E.; Stensgaard, I.; Brune, H.; Besenbacher, F. High-coverage structures of carbon monoxide adsorbed on Pt(111) studied by high-pressure scanning tunneling microscopy. *J. Phys. Chem. B* **2004**, *108*, 14497–14502.
- (35) Böller, B.; Zeller, P.; Günther, S.; Wintterlin, J. High-pressure CO phases on Co(0001) and their possible role in the Fischer—Tropsch synthesis. *ACS Catal.* **2020**, *10*, 12156–12166.

